Microwave Characterization of Josephson Junction Arrays: Implementing a Low Loss Superinductance

Nicholas A. Masluk,[*] Ioan M. Pop, Archana Kamal, Zlatko K. Minev, and Michel H. Devoret

Department of Applied Physics, Yale University, 15 Prospect Street, New Haven, Connecticut 06511, USA
(Received 21 June 2012; published 27 September 2012)

We have measured the plasma resonances of an array of Josephson junctions in the regime $E_J \gg E_C$, up to the ninth harmonic by incorporating it as part of a resonator capacitively coupled to a coplanar waveguide. From the characteristics of the resonances, we infer the successful implementation of a superinductance, an electrical element with a nondissipative impedance greater than the resistance quantum $[R_Q = h/(2e)^2 \simeq 6.5 \text{ k}\Omega]$ at microwave frequencies. Such an element is crucial for preserving the quantum coherence in circuits exploiting large fluctuations of the superconducting phase. Our results show internal losses less than 20 ppm, self-resonant frequencies greater than 10 GHz, and phase-slip rates less than 1 mHz, enabling direct application of such arrays for quantum information and metrology. Arrays with a loop geometry also demonstrate a new manifestation of flux quantization in a dispersive analog of the Little-Parks effect.

The emerging field of quantum electronics exploiting large fluctuations of the superconducting phase is challenged by the engineering of an electromagnetic environment which suppresses simultaneously the quantum fluctuations of charge and the random low-frequency fluctuations of offset charges. The small value of the fine structure constant $\alpha = 1/137$ entails a fundamental asymmetry between flux and charge quantum fluctuations, strongly favoring the latter. To illustrate this, let us consider the simplest case of a dissipationless LC oscillator, where the charge Q on the capacitor plates and the generalized flux Φ across the inductor are conjugate variables. The ratio between quantum fluctuations of charge, $\delta q = \delta Q/(2e)$, and flux, $\delta\varphi = \delta\Phi/\Phi_0$, in the ground state of the oscillator is given by $\delta\varphi/\delta q = Z_0/R_Q$. Here $Z_0 = \sqrt{L/C}$ is the characteristic impedance of the oscillator and $R_Q = h/(2e)^2 = 6.5 \text{ k}\Omega$ is the superconducting resistance quantum. Using only geometrical inductors and capacitors, the characteristic impedance of the oscillator Z_0 cannot exceed the vacuum impedance $Z_{\text{vac}} = \sqrt{\mu_0/\epsilon_0}$, thus imposing quantum fluctuations of charge at least an order of magnitude larger than flux fluctuations: $\delta q/\delta\varphi > R_Q/Z_{\text{vac}} = 1/(8\alpha)$.

On-chip resistors and long chains of Josephson junctions (JJs) in the dissipative regime have already been used to provide high impedance environments for the phase across a Josephson element [1–3]. However, these Ohmic components cannot screen charge offsets efficiently and, being dissipative, tend to destroy the quantum coherence of the devices. We thus need a circuit element which possesses three key attributes: high impedance at frequencies of interest, perfect conduction at DC, and extremely low dissipation. These attributes define the so-called "superinductance" [4,5].

There are currently two leading candidates for implementing superinductances. The first is superconducting nanowires [6,7]. Unfortunately, they appear to show significant internal dissipation, which is not yet well understood, and they are challenging to fabricate. The second implementation exploits the large kinetic inductance of arrays of JJs. Though amenable to design parameters, arrays may also suffer from dissipation due to coupling to internal degrees of freedom [8,9] or to coupling to a dissipative external bath [10]. Indeed, transport measurements on large arrays of JJs show the appearance of a superconducting to insulating transition (SIT) with decreasing Josephson energy E_J [11–13]. Previous measurements on resonators where the inductive energy is dominated by JJ arrays have yielded internal quality factors in the range of a few thousands [14,15]. The long lifetime of the fluxonium qubit was the first indirect evidence of a low-loss superinductance based on JJ arrays [5,16]. However, this realization suffered from coherent quantum phase slips (CQPS) [17,18], which constitute additional degrees of freedom, difficult to control experimentally.

In this Letter, we report microwave characterization of arrays of large JJs [see Fig. 1(a)] with Josephson energy $E_J \simeq 180E_C$, where $E_C = e^2/(2C_J)$ is the charging energy of one junction. The parasitic capacitance of the array to ground is such that the CQPS rate is exponentially suppressed with E_J/E_C [19].

Our arrays consist of closely spaced Josephson junctions on a C-plane sapphire substrate, as shown in Fig. 1. We fabricated the junctions by e-beam lithography and double angle evaporation of aluminum using the bridge-free technique of [20,21]. Prior to aluminum deposition, the substrate is cleaned of resist residues using an oxygen plasma [22]. We minimize the width of the connecting wires between junctions in order to reduce parasitic capacitances
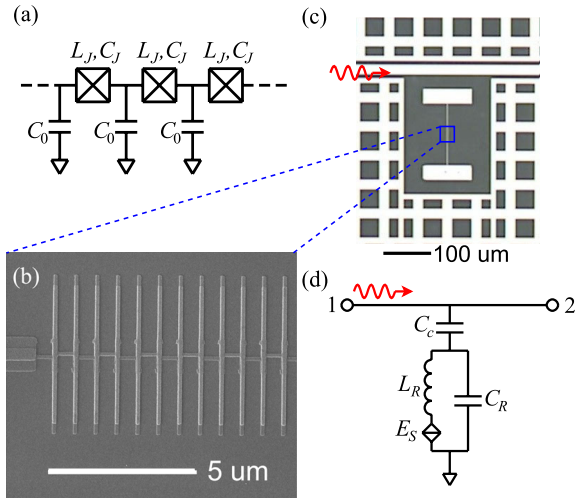
FIG. 1 (color online). (a) Schematic representation of an array of Josephson junctions. Capacitances of islands to ground and across tunnel junctions are denoted with C_0 and C_J, respectively. The junction inductance is given by L_J. (b) SEM image of the Josephson junction array fabricated using the bridge-free technique [20,21]. (c) Optical image of an LC resonator. The large pads implement the resonator capacitance as well as coupling capacitances to the coplanar waveguide feedline. An array of Josephson junctions between the pads implements the superinductance. The ground plane is patterned with flux-trapping holes. (d) Low-frequency model for the device shown in (c). The phase-slip element (split diamond) in series with the superinductance represents the collective contribution of phase slips through all junctions in the array. The characteristic energy of the phase-slip element is denoted by E_S.

to ground, which ultimately lower the self-resonant frequency of the superinductance [23].

We characterize our superinductances at low temperatures and microwave frequencies by incorporating them in lumped-element LC resonators capacitively coupled to a coplanar waveguide in the hanger geometry. The resonator response is measured in transmission. An optical image of a typical device and its low-frequency circuit model are shown in Figs. 1(c) and 1(d).

The samples were mounted on the mixing chamber stage (15 mK) of a dilution refrigerator inside a copper box, enclosed in an aluminum-Cryoperm-aluminum shield with a Cryoperm cap. We used two 4–12 GHz Pamtech isolators and a 12 GHz K&L multisection low-pass filter before the HEMT amplifier, and installed copper powder filters on the input and output lines.

The internal quality factor of a resonator is extracted by fitting the transmission data about the resonance with the response function [24]

$$S_{21}(f) = 1 - \frac{Q_{\text{ext}}^{-1} - 2i\frac{\delta f}{f_R}}{Q_{\text{tot}}^{-1} + 2i\frac{f-f_R}{f_R}}, \qquad (1)$$

where Q_{tot} and Q_{ext} are the total and external quality factors, f_R is the resonant frequency, and δf characterizes asymmetry in the transmission response profile. The internal quality factor is given by $Q_{\text{int}} = \frac{Q_{\text{ext}} Q_{\text{tot}}}{Q_{\text{ext}} - Q_{\text{tot}}}$. We show a typical measured response for a resonator with an 80-junction superinductance in Fig. 2(a). This yields an internal quality factor of 37 000 for the resonator at 15 mK (stage temperature), corresponding to a loss in the superinductance of better than 27 ppm. We note that an unknown portion of the internal loss comes from the capacitors. The inset of Fig. 2(a) shows the dependence of the internal quality factor on the stage temperature. The quality factor appears to saturate at low temperatures; this can either indicate the presence of nonequilibrium quasiparticles, or more likely the approach of the noise floor of our measurement setup, limiting the resolvable values for the Q. A similar resonator with two 80-junction arrays in parallel was measured to have a quality factor of 56 000 [Fig. 2(b)], corresponding to a superinductance loss of smaller than 18 ppm, an order of magnitude below the previously reported values [14]. The external quality factors, Q_{ext}, of both resonators were 5000.
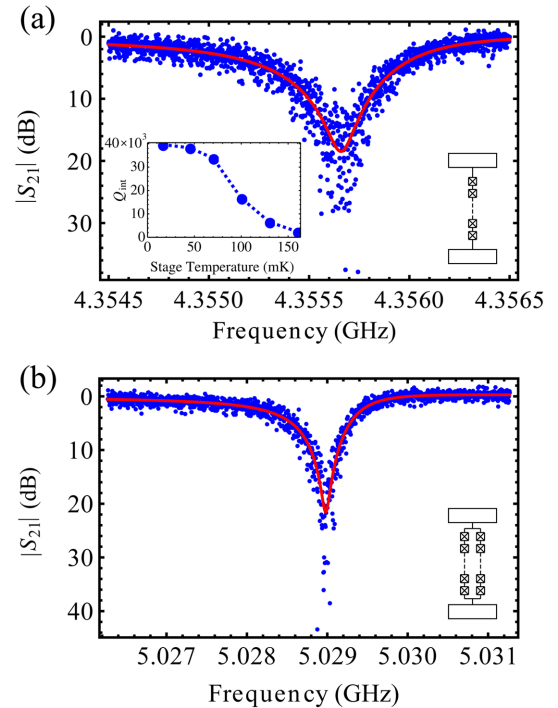
FIG. 2 (color online). (a) Typical microwave transmission data for an 80-junction resonator measured with order one photon circulating power; the solid line is the theoretical prediction corresponding to $Q_{\text{int}} > 37\,000$. Inset: Temperature dependence of the internal quality factor of the resonator. The dashed line is a guide for the eye. (b) Same measurement as in (a) for a 160-junction array loop; the solid line corresponds to $Q_{\text{int}} > 56\,000$. Parameters for the low-frequency model in Fig. 1(d) are $C_c = 1.6$ fF, $C_R = 7.2$ fF, and $L_R = 150$ nH for (a) and $C_c = 1.8$ fF, $C_R = 11$ fF, and $L_R = 76$ nH for (b).

We next evaluate the self-resonant modes of an
N-junction array. The Lagrangian of the array is

$$\mathcal{L} = \sum_{n=1}^{N} \frac{1}{2} C_0 \dot{\Phi}_n^2 + \frac{1}{2} C_J (\dot{\Phi}_n - \dot{\Phi}_{n+1})^2$$
$$- \frac{1}{2} \frac{(\Phi_n - \Phi_{n+1})^2}{L_{J0}}, \qquad (2)$$

where Φ_n are the node fluxes associated with each super-
conducting island. We express each node flux as a super-
position of discrete Fourier mode amplitudes,

$$\Phi_n = \frac{1}{\sqrt{N}} \sum_{k=1}^{N} e^{i(\pi k/N)n} \Phi_k, \qquad (3)$$

which leads to a diagonal Hamiltonian of the following
form:

$$\mathcal{H} = \sum_{k=-N/2}^{N/2} \mathbb{C}_{kk'}^{-1} Q_k Q_{-k'} + \mathbb{L}_{kk'}^{-1} \Phi_k \Phi_{-k'}. \qquad (4)$$

Here Q_k are the canonical conjugate "charge" variables
to the fluxes Φ_k, and

$$\mathbb{C}_{kk'} = \delta_{kk'} \left[\frac{C_0}{2} + C_J \left(1 - \cos \frac{\pi k}{N} \right) \right]; \qquad k \in \left[-\frac{N}{2}, \frac{N}{2} \right] \qquad (5)$$

$$\mathbb{L}_{kk'} = \delta_{kk'} \frac{L_{J0}}{\left(1 - \cos \frac{\pi k}{N} \right)}, \qquad (6)$$

are respective capacitance and inductance matrices in the
Fourier basis. This immediately leads to a dispersion rela-
tion of the form

$$\omega_k = (L_{kk} C_{kk})^{-1/2} = \omega_0 \sqrt{\frac{1 - \cos \frac{\pi k}{N}}{\frac{C_0}{2C_J} + \left(1 - \cos \frac{\pi k}{N} \right)}}, \qquad (7)$$

where $\omega_0 = 1/\sqrt{L_J C_J}$ is the plasma frequency of a single
junction. The coupling capacitance pads at each end of the
array [see Fig. 1(c)] load down the eigenfrequencies (see
Supplemental Material [25] for calculation details).

The data presented in Fig. 2 correspond to measure-
ments of the $k = 1$ mode. The frequencies of higher
modes, $k \geq 2$, of the array lie outside the band of our
measurement setup. In order to observe these modes we
exploit their cross-Kerr interaction, which is induced by
the junction nonlinearity. This interaction leads to a fre-
quency shift of the lowest mode ($k = 1$) when higher
modes are excited. In Fig. 3(a) we show the results of a
two-tone measurement of an 80-junction resonator [same
device as presented in Fig. 2(a)], where we continuously
monitor the $k = 1$ mode while sweeping the frequency of a
probe tone. When the probe tone is resonant with a higher
mode of the array, we observe a drop in the $k = 1$
frequency.
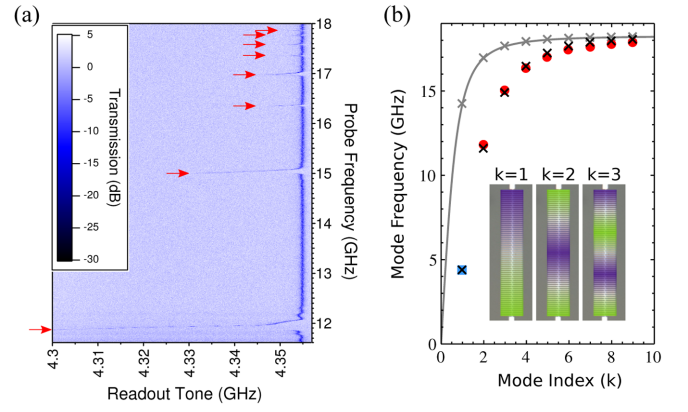
FIG. 3 (color online). (a) Shift of the lowest frequency mode of
the 80-junction resonator upon application of a probe tone.
Because of the weak nonlinearity of the array (theory predicts
of order 10 MHz/photon [33]), shifts occur when the probe tone
matches a plasmonic resonance of the array (marked with
red arrows). (b) Measured plasma mode frequencies of the
80-junction array: The blue square represents the fundamental
resonant frequency of the resonator (4.355 GHz), and red circles
indicate the plasma modes pointed out by red arrows in (a). The
black crosses denote the calculated plasma frequencies. The
gray curve represents the dispersion relation without including cor-
rections due to the coupling capacitors (open boundary condi-
tions), and markers show corresponding plasma frequencies. The
inset in (b) shows the voltage profile along the array for the first
three plasma modes.

Figure 3(b) shows the comparison between the mea-
sured frequencies of the array modes and the theoreti-
cally predicted values. The black crosses show the
renormalized mode frequencies calculated after incorpo-
ration of the corrections due to coupling capacitance
pads (see Supplemental Material [25]), which are in
good agreement with the measured frequencies repre-
sented by colored markers. The parameters extracted
from the fit were $C_0 = 0.04$ fF, $C_J = 40$ fF, and $L_J =
1.9$ nH, with a confidence range of 20%. The simulated
value of the capacitance to ground $C_0 = 0.09$ fF agrees
within a factor of 2 with the inferred value from the fit.
Room temperature resistance measurements of the junc-
tion arrays yield a value of $L_J = 2.1$ nH, which agrees
with the fit within 10%. Using the fit parameters we
calculate the dispersion relation for the bare superinduc-
tance, shown as a gray curve in Fig. 3(b). We note that
the lowest resonant frequency of the bare superinduc-
tance is 14.2 GHz, which meets the design criterion of
having self-resonances well above the frequency range of
interest (1–10 GHz).

In order to characterize the phase-slip rate of the super-
inductances, we monitor the frequency of the $k = 1$ mode
of a resonator formed by two superinductances in parallel,
while sweeping an external magnetic field. As flux bias is
increased, the persistent current induced in the loop in-
creases, and results in a drop in frequency of the mode
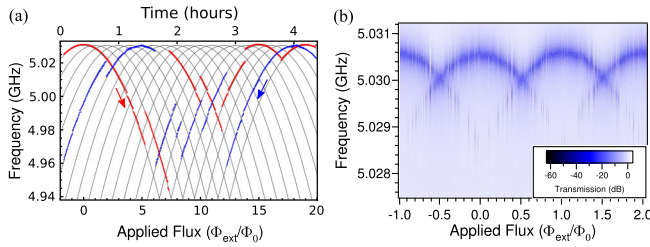
FIG. 4 (color online).   (a) Lowest mode frequency versus applied flux bias for resonator with 160-junction array loop. Flux bias is swept up and down over the course of several hours. Gray curves represent quasiclassical predictions for resonator frequencies at different integer values of flux quanta in the array loop. The only adjustable parameter is the number of junctions, found to be 150 ± 10. (b) Same measurement as in (a) over a smaller flux range, but before each measurement a high power pulse at one of the plasma modes is applied in order to reset the resonator to the lowest flux state.

[Fig. 4(a)]. This behavior can be described to lowest order in junction nonlinearity by the quasiclassical expression

$$f(\Phi_{\mathrm{ext}}) = \frac{f_R}{\sqrt{1 + \frac{1}{2}\left[\frac{2\pi}{N}\left(\frac{\Phi_{\mathrm{ext}}}{\Phi_0} - m\right)\right]^2}}, \qquad (8)$$

where Φ_{ext} is the applied flux bias, and m is the integer number of flux quanta inside the loop. A phase-slip event is associated with an integer change in m, which we observe as a jump in resonator frequency. As we increase the flux bias, the phase-slip rate is enhanced and frequency jumps become more probable [19]. We swept the flux bias applied to the loop over several flux quanta before a phase-slip event occurred. The typical duration between phase slips recorded in this experiment was over an hour, Fig. 4(a). This is a remarkably low phase-slip rate of well under 1 mHz for a loop of 160 junctions, significantly lower than previously reported values on shorter arrays [17,26].

Because of the extremely low phase-slip rate, in order to measure the resonator in the lowest flux state, we employ an active resetting scheme. We apply a high power pulse at one of the $k \geq 2$ modes before measuring the location of the lowest resonant frequency. This high power pulse activates phase slips, relaxing the loop to the lowest flux state. Remarkably this allows a change in persistent current at constant flux bias. Using this protocol, we tracked the resonant frequency in the lowest flux state, as shown in Fig. 4(b), and observed discrete inverted parabolas. This periodic modulation of the resonator frequency with flux is akin to the Little-Parks effect [27] measured dispersively in a nondissipative regime. We exploit this effect to unambiguously calibrate the number of flux quanta in the loop. The fitted value for the total number of junctions differs by 6% from the actual number, which can be explained by the classical nature of the theory which does not take quantum fluctuations into account.

In conclusion, microwave measurements of superconducting Josephson junction arrays demonstrate that superinductances in the range of 100–300 nH, with self-resonant frequencies above 10 GHz, internal losses less than 20 ppm, and phase-slip rates below 1 mHz can be successfully implemented. With parameters such as measured in our experiment, Josephson junction array superinductances significantly enrich the quantum electronics toolbox. Applications would include further suppression of offset charges in superconducting qubits [16], high Q and tunable lumped-element resonators, on-chip bias tees, and kinetic inductance particle detectors [28]. In addition, these arrays exhibit rich dynamics owing to many internal degrees of freedom, thus making them perfect candidates for the study of quantum many-body phenomena such as quantum impurity models [29,30], microwave photonics [31], and measurements of Bloch oscillations [32].

*nicholas.masluk@yale.edu
[1] L. S. Kuzmin and D. B. Haviland, Phys. Rev. Lett. **67,** 2890 (1991).
[2] S. V. Lotkhov, S. A. Bogoslovsky, A. B. Zorin, and J. Niemeyer, Phys. Rev. Lett. **91,** 197002 (2003).
[3] S. Corlevi, W. Guichard, F. W. J. Hekking, and D. B. Haviland, Phys. Rev. Lett. **97,** 096802 (2006).
[4] Term introduced by A. Kitaev (unpublished).
[5] V. E. Manucharyan, Ph.D. thesis, Yale University, New Haven, Connecticut, 2011.
[6] A. Bezryadin, C. N. Lau, and M. Tinkham, Nature (London) **404,** 971 (2000).
[7] J. E. Mooij and Y. V. Nazarov, Nature Phys. **2,** 169 (2006).
[8] R. Fazio and H. van der Zant, Phys. Rep. **355,** 235 (2001).
[9] G. Rastelli, I. M. Pop, W. Guichard, and F. W. J. Hekking, arXiv:1201.0539.
[10] A. M. Lobos and T. Giamarchi, Phys. Rev. B **84,** 024523 (2011).
[11] E. Chow, P. Delsing, and D. B. Haviland, Phys. Rev. Lett. **81,** 204 (1998).
[12] W. Kuo and C. D. Chen, Phys. Rev. Lett. **87,** 186804 (2001).
[13] Y. Takahide, H. Miyazaki, and Y. Ootuka, Phys. Rev. B **73,** 224503 (2006).
[14] M. A. Castellanos-Beltran and K. W. Lehnert, Appl. Phys. Lett. **91,** 083509 (2007).

[15] A. Palacios-Laloy, F. Nguyen, F. Mallet, P. Bertet, D. Vion, and D. Esteve, J. Low Temp. Phys. **151,** 1034 (2008).

[16] V. E. Manucharyan, J. Koch, L. I. Glazman, and M. H. Devoret, Science **326,** 113 (2009).

[17] V. E. Manucharyan, N. A. Masluk, A. Kamal, J. Koch, L. I. Glazman, and M. H. Devoret, Phys. Rev. B **85,** 024521 (2012).

[18] I. M. Pop, B. Douçot, L. Ioffe, I. Protopopov, F. Lecocq, I. Matei, O. Buisson, and W. Guichard, Phys. Rev. B **85,** 094503 (2012).

[19] K. A. Matveev, A. I. Larkin, and L. I. Glazman, Phys. Rev. Lett. **89,** 096802 (2002).

[20] F. Lecocq, I. M. Pop, Z. Peng, I. Matei, T. Crozes, T. Fournier, C. Naud, W. Guichard, and O. Buisson, Nanotechnology **22,** 315302 (2011).

[21] C. T. Rigetti, Ph.D. thesis, Yale University, New Haven, Connecticut, 2009.

[22] I. M. Pop, T. Fournier, T. Crozes, F. Lecocq, I. Matei, B. Pannetier, O. Buisson, and W. Guichard, J. Vac. Sci. Technol. B **30,** 010607 (2012).

[23] C. Hutter, E. A. Tholén, K. Stannigel, J. Lidmar, and D. B. Haviland, Phys. Rev. B **83,** 014511 (2011).

[24] K. Geerlings, S. Shankar, E. Edwards, L. Frunzio, R. J. Schoelkopf, and M. H. Devoret, Appl. Phys. Lett. **100,** 192601 (2012).

[25] See Supplemental Material at http://link.aps.org/supplemental/10.1103/PhysRevLett.109.137002 for information on the simulation of parasitic capacitance, calculation of the hanger geometry scattering matrix, fabrication, and calculations of the modification of array mode frequencies by coupling pad capacitances.

[26] I. M. Pop, I. Protopopov, F. Lecocq, Z. Peng, B. Pannetier, O. Buisson, and W. Guichard, Nature Phys. **6,** 589 (2010).

[27] W. A. Little and R. D. Parks, Phys. Rev. Lett. **9,** 9 (1962).

[28] P. K. Day, H. G. LeDuc, B. A. Mazin, A. Vayonakis, and J. Zmuidzinas, Nature (London) **425,** 817 (2003).

[29] K. Le Hur, Phys. Rev. B **85,** 140506 (2012).

[30] M. Goldstein, M. H. Devoret, M. Houzet, and L. I. Glazman, arXiv:1208.0319.

[31] D. Zueco, J. J. Mazo, E. Solano, and J. J. García-Ripoll, Phys. Rev. B **86,** 024503 (2012).

[32] W. Guichard and F. W. J. Hekking, Phys. Rev. B **81,** 064508 (2010).

[33] I. Pop *et al.* (unpublished).

[34] M. T. Bell, I. A. Sadovskyy, L. B. Ioe, A. Y. Kitaev, and M. E. Gershenson, following Letter, Phys. Rev. Lett. **109,** 137003 (2012).